
Article:
Cook, J.M., Edwards, A., Bulling, M. et al. (2016) Metabolome-mediated biocryomorphic evolution promotes carbon fixation in Greenlandic cryoconite holes. Environmental Microbiology, 18. pp. 4674-4686. ISSN: 1462-2912

https://doi.org/10.1111/1462-2920.13349

Metabolome-mediated biocryomorphic evolution promotes carbon fixation in Greenlandic cryoconite holes

Cook, J.M[1,2]., Edwards, A[3]*., Bulling, M[2]., Mur, L.A.J[3], Cook, S[3]., Gokul, J.K.[3], Cameron, K.A[4,5]., Sweet, M[2]., Irvine-Fynn, T.D.L[6].

[1]*Department of Geography, University of Sheffield, Sheffield, UK, S10 2TN*

[2] *College of Life and Natural Sciences, University of Derby, UK, DE22 1GB*

[3] *Institute of Biological, Environmental and Rural Sciences, Aberystwyth University, SY23 3DA*

[4]*Department of Geochemistry, Geological Survey of Denmark and Greenland (GEUS), 1350 Copenhagen, Denmark*

[5]*Center for Permafrost (CENPERM), University of Copenhagen, 1350 Copenhagen, Denmark*

[6]*Centre for Glaciology, Department of Geography and Earth Sciences Aberystwyth University, SY 23 3DA*

**Corresponding author:*

**Corresponding Author: E-mail: aye@aber.ac.uk Arwyn Edwards. Institute of Biological, Rural and Environmental Sciences, Cledwyn Building, Aberystwyth University, Aberystwyth, SY23 3FG, UK. +44(0)1970 622330*

Keywords: Metabolomics / Greenland / Cryoconite / Autotrophy / Biocryomorphic evolution

Running title: Biocryomorphic evolution of cryoconite holes

Originality-Significance Statement:

Cryoconite holes are microbially-engineered habitats where phototrophic microbe-mineral aggregates darken glacial ice. We show the consequent habitat structure reciprocally controls solar energy receipt and thus promotes microbial photoautotrophy. Moreover, perturbation of energy receipt incurs profound changes in the cryoconite metabolome mediated by cAMP signalling and fucose catabolism, promoting resilience in primary productivity. Our study reveals how biocryomorphic microbial interactions self-regulate the accumulation of autochthonous organic matter, with implications for carbon cycling and melting of the climatically-sensitive margin of the Greenland Ice Sheet.

Summary: (199 words)

Microbial photoautotrophs on glaciers engineer the formation of granular microbial-mineral aggregates termed cryoconite which accelerate ice melt, creating quasi-cylindrical pits called 'cryoconite holes'. These act as biogeochemical reactors on the ice surface and provide habitats for remarkably active and diverse microbiota. Evolution of cryoconite holes towards an equilibrium depth is well known, yet interactions between microbial activity and hole morphology are currently weakly addressed. Here, we experimentally perturbed the depths and diameters of cryoconite holes on the Greenland Ice Sheet. Cryoconite holes responded by sensitively adjusting their shapes in three dimensions ('biocryomorphic evolution') thus maintaining favourable conditions for net autotrophy at the hole floors. Non-targeted metabolomics reveals concomitant shifts in cyclic AMP and fucose metabolism consistent

with phototaxis and extracellular polymer synthesis indicating metabolomic-level granular changes in response to perturbation. We present a conceptual model explaining this process and suggest that it results in remarkably robust net autotrophy on the Greenland ice sheet. We also describe observations of cryoconite migrating away from shade, implying a degree of self-regulation of carbon budgets over mesoscales. Since cryoconite is a microbe-mineral aggregate, it appears that microbial processes themselves form and maintain stable autotrophic habitats on the surface of the Greenland ice sheet.

Introduction:

Glaciers represent spatially-expansive and vulnerable microbial ecosystems (Hodson et al 2008). On bare ice, filamentous photoautotrophs entangle allochthonous organic and inorganic matter to form discrete granules termed cryoconite (Takeuchi et al., 2010; Langford et al., 2010; Cook et al, 2015a). Cryoconite granules provide stable microhabitats for communities of autotrophic and heterotrophic microbes concentrating biodiversity, carbon and nutrient cycling on ice surfaces (Phillipp, 1912; Kohshima et al., 1987; Hodson et al., 2008). Microbial cementation of organic matter by extracellular polymeric substances has previously been identified as a form of autogenic engineering (Langford et al., 2010; Edwards et al., 2014), analogous to aggregation processes in desert soils (West et al., 1990; Six et al., 2004). Since cryoconite is a prominent habitat within the expansive and expanding region of the Greenland ice sheet surface which is biologically productive in summer (occupying 1-7% of the surface of an area >200,000 km^2; Hodson et al., 2010; Cook et al. 2012), the impacts of granule-scale changes have consequences at much larger scales.

As well as stabilising granules, the microbial processes darken them and increase their efficiency as conductors of thermal energy. Patches of cryoconite granules therefore locally accelerate ice surface melt, driving the formation of quasi-cylindrical pits called 'cryoconite holes' (e.g. Wharton et al, 1985). The morphology of cryoconite holes is primarily controlled

by light intensity and sediment supply (Gribbon, 1979; McIntyre, 1984; Wharton et al, 1985; Cook et al., 2010); however, hole morphology also reciprocally controls hole floor irradiance. During periods of greater irradiance, holes deepen, presumably maintaining relatively constant irradiance at the hole floor (Gribbon, 1979). Due to their thermal conductivity, thick layers of cryoconite granules enhance the melting of cryoconite hole walls, widening the holes and spreading the granules out to minimise granule overlapping (commonly forming single-grain layers, *hereafter* 'SGL'). The effect of this is to expose the maximum photosynthetically active surface area of the granules to incoming solar irradiance (Cook et al., 2010). Therefore, since autotrophy in cryoconite is overwhelmingly dominated by photosynthesis (Cook et al., 2010; Telling et al., 2012), hole morphology likely regulates the net ecosystem productivity (NEP) on the hole floor, possibly providing an important source of labile organic carbon (OC) for downstream ecosystems including streams, lakes and oceans (e.g. Wilhelm et al., 2013; Hood et al., 2009; Lawson et al., 2014).

While cryoconite bacterial community structure correlates with community metabolomes (Edwards et al. 2014), interactions between hole morphology and sediment layers will change over briefer timescales than those permitting changes in community structure, considering the prolonged and community doubling times (Anesio et al. 2010) and apparent taxonomic temporal stability of Greenlandic cryoconite communities (Musilova et al. 2015; Stibal et al. 2015). This implies that community responses occur via metabolic adaptations rather than taxonomic shifts, necessitating a metabolomic perspective on interactions between the cryoconite microbiota and their habitat.

Since the regulation of hole morphology is a biologically mediated process driven by granule formation and darkening, and the result is likely stabilisation of favourable conditions for autotrophy on the hole floors, we contend the three dimensional evolution of hole shapes entails what may be termed 'biocryomorphic' evolution. This can be thought of as the

propagation of autogenic ecosystem engineering of granule microhabitats through to the shaping of the ice surface at the scale of individual cryoconite holes. Conditions typically experienced by cryoconite holes in the ablation zone of the south-western Greenland Ice Sheet, namely high levels of irradiance coupled with slower moving low-gradient ice provide a natural laboratory for testing this hypothesis (Cook et al., 2015b).

In this study we examined whether cryoconite hole morphology responds to environmental disturbances and regulates the carbon budgets and metabolomes of incumbent microbiota. We reasoned that there are two major environmental controls upon cryoconite carbon fluxes, the first being reduced incident radiation due to topographic shading, cloud cover or low solar angle at the ends of melt seasons, the second being overlapping of cryoconite granules following sediment delivery into the holes. Therefore, two separate experiments were established: one used filter screens to limit the incident radiation entering cryoconite holes; the other artificially thickened the sediment layers in initially stable holes. Hole morphology, rates of NEP and community metabolomes were then monitored daily over seven days.

Results:

Depth evolution: Morphology

We assessed the morphological and carbon flux responses of cryoconite holes to disturbances to their equilibrium depths. The intensity of solar radiation entering cryoconite holes was varied using filter screens, dramatically changing their depths (Figure 1). Holes under the stronger of the two filters lost most depth over the observation period (181.3 mm ± 9.3 mm (S.E.)) followed by those under the weaker filter (113mm ± 0.33 mm (S.E.)). Significant negative linear trends were observed in the depths of the holes under both filters over the measurement period (linear regression: r^2= 0.96, F= 108.71, p=0.0001 for the weaker filter; r^2= 0.94, F= 79.71, p= 0.0003 for the stronger filter, see Supplementary Table 1). No

statistically significant trend was observed in the depths of a control group of holes (r^2= 0.53, F= 5.84, p = 0.06) (Supplementary Table 1). The final depths of holes in each light regime were all significantly different (paired t-tests, p< 0.001), with the mean depths on the final day of observation being 31 ± 1 mm (S.E) under the stronger filter, 78 ± 4 mm (S.E.) under the weaker filter and 153 ± 0.8 mm (S.E.) in the control holes. In both filtered sets of holes the decrease in mean hole depth over the measurement period was best described by logarithmic functions (r^2 = 0.978, F = 216.7, p <0.0001, for the weaker filter, and r^2 = 0.991, F = 563.4, p <0.0001, for the stronger filter).

Depth evolution: Carbon cycling

NEP rates in cryoconite in the different light regimes converged over the measurement period (Figure 1). In both groups of filtered holes significant linear trends in NEP were recorded (Supplementary Table 1), shifting from initial net heterotrophy to final net autotrophy (Figure 1). Mean NEP under the weaker filter decreased by 3.74 ± 0.81 μg C g^{-1} d^{-1}, compared to 4.65 ± 0.9 μg C g^{-1} d^{-1} under the stronger one. Cryoconite under the stronger filter was consistently the most heterotrophic and took longer to become net autotrophic (5 days, compared to just 2 days under the weaker filter). In the filtered holes significant positive correlations were found between hole depth and NEP (Pearson's: R = 0.93, p = 0.009 and R= 0.91, p= 0.01 for weaker and stronger filters respectively). No significant trends in NEP were observed in the control holes or incubations placed directly upon the ice surface, both of which maintained relatively stable net autotrophy (Figure 1; Supplementary Table 1). Cryoconite incubated on the ice surface sequestered more carbon than any of the other sets of incubations throughout the experiment with the exception of day 1 when natural cryoconite was more strongly net autotrophic (Figure 1). Respiration measured in dark incubations was relatively constant at 26.83 – 28.03 μg C g^{-1} d^{-1} throughout the measurement period, showing no significant trends (linear regression, r^2 =0.29, F = 1.67, p = 0.27 for surface incubations; r^2

=0.01, F = 0.83, p = 0.05 for control holes; r^2 = 0.02, F = 0.79, p = 0.08 for holes shaded by the weaker filter; r^2 =0.36, F = 2.28, p = 0.2 for holes shaded by the stronger filter).

Planform evolution: Morphology

The second experiment monitored NEP and hole shapes in plan-view following artificial 'overloading' of cryoconite holes with excess cryoconite granules. A dramatic widening of all of the overloaded holes occurred (Fig 1; Fig 2) with average widths (measured across two perpendicular axes) increasing linearly (Supplementary Table 2) from starting values of 215.5, 177.5 and 268.5 mm to end values of 522.5, 395 and 515 mm for holes 1, 2 and 3 respectively. This widening initiated at the interface between cryoconite and hole wall and was sustained throughout the observation period, undercutting hole walls (as illustrated in supplementary information. 1E and 1F). Over time, the extent of undercutting increased, plateaued and finally diminished as surface ablation erased the relict hole profile (Figure 1). As the holes widened there was a simultaneous change in the distribution of cryoconite on the hole floor (Figure 2). Initially, layers of cryoconite thinned only at the periphery, forming an outer ring of displaced granules separated from the main central bulk of cryoconite by a clear escarpment (or 'scarp'), indicating translational sliding of material downslope (Figure 3A). This scarp was arranged in a ring, and will hereafter be referred to as the "equilibrium ring" (ER). The ER initially contracted towards the centre of the hole, separating an expanding periphery of thin, well-spread cryoconite from a shrinking interior zone of stacked cryoconite (Figure 3A). Simultaneously, hole floors outside of the ER steepened to a maximum of at least 35° (measured in Hole 1 on 27th July). Continued downslope movement outside of the ER maintained contact between multi-grain layers (MGL) of granules and the hole walls, sustaining melt. In the latter half of the observation period, sediment ceased to thin from the periphery and instead thinned from the centre (Figure 2; Fig 3B). During this later period, the hole floor flattened, resulting in a near ubiquitous SGL in all of the overloaded holes (Figure

2). Interestingly, Hole 1 showed a strong tendency to expand northwards (Figure 2), in contrast with the other two holes which expanded remarkably symmetrically (Figure 2). This included a northwards shift in the sediment contained within the hole (as evidenced by a 150 mm northwards migration of the hole's centroid: Figure 3) and asymmetric planform evolution strongly favouring the advance of the south facing wall (300 mm displacement compared to 120 mm for the north-facing wall). Hole 1 was shaded by a slight topographic rise to the south, which probably explains this behaviour. Movies of the plan-view and cross-sectional evolution of the cryoconite layers are presented in supplementary information 2 and 3 respectively.

The depths of all the studied holes changed simultaneously to the evolution of their planforms (Supplementary Table 2). In Hole 1, depth evolution was linear until the 27th July (r^2 = 0.88, F= 61.14, p <0.0001), after which the trend was obscured by the development of a complex hole floor topography. A significant linear decrease in the depth of Hole 2 was also observed (r^2 = 0.90, F= 136.15, p <0.0001); however it was better described using a logarithmic curve (r^2 = 0.93, F=176.6, p<0.0001). Hole 2 gradually became shallower (by 75 mm) over the observation period. In contrast, Hole 3 showed a linear decrease in depth (linear regression, r^2 = 0.91, F = 92, p <0.0001) to a minimum of 267 mm on 28th July, before deepening again logarithmically (r^2 = 0.87, F=28.32, p <0.0001) on the 29th to a plateau at 300 mm. Despite the contrasting depth evolution between the holes, their width:depth ratios all increased linearly over the measurement period (Supplementary Table 2).

Planform evolution: Carbon cycling

NEP at distance 'x' from the centre of each hole was found to be net heterotrophic between 1-5 days after overload (Figure 1). During this period the radius of the ER exceeded that of x. After 5 days, the ER in all three holes had contracted past x, and mean NEP showed a rapid decrease (as evidenced by the linear regression: r^2 = 0.92, F = 23.41, p = 0.04). Holes 1 and 3

became net autotrophic on day 7, while Hole 2 became net autotrophic on day 6. Mean respiration measured in dark incubations was relatively constant between 24.6 and 26.2 μg C g^{-1} d^{-1} throughout the measurement period (linear regression, $r^2 = 0.1$, F= 0.56, p= 0.49).

Non-targeted Metabolomics

Metabolite extracts from triplicate sediment samples from each cryoconite hole on each day in the sediment overloading experiment and single samples (with triplicate samples on the final day) of the depth evolution experiment were processed using mass spectrometry. Hierarchical Cluster Analysis (HCA; Figure 4A) of the overloading experiment shows higher relative concentrations of metabolites in heterotrophic conditions with a clear shift concomitant with the transition from net heterotrophy to net autotrophy. Hierarchical Cluster Analysis (HCA) and Principal Component Analysis (PCA) both confirmed the distinctive metabolome profiles of the Day 8 samples (supplementary information. 5) with the major sources of variation as indicated by the PC1 Loading vectors (Figure 4B). Comparisons with databases and mass-ion standards indicated that the metabolites driving a temporal model were changes in fucose, cyclic AMP (cAMP), dichlorophenol and uridine monophosphate (UMP). MS measurements linked to fucose (Figure 4C) or cAMP (Figure 4D) metabolism were extracted from the data matrix and interrogated in discrete HCA. In both biochemical pathways, temporal changes in metabolites matched those of the whole detected metabolome (Figure 4A), suggesting transient increases in the key signalling molecule cAMP as well as fucose metabolism leading to the generation of pyruvate to feed into the tricarboxylic acid cycle and / or gluconeogenesis or anaerobic metabolism linked to the production of lactate. The link with lactate was strongly suggested by the highly significant Pearson's correlations observed between lactate and fucose metabolites (Figure 4E). The correlations between adenosine nucleotides and cAMP were also highly significant, consistent with a shift of nucleotide metabolism towards the generation of this signal. To explore the generality of

metabolomic responses, samples collected from the depth evolution experiment were also examined. The limited temporal replication of metabolite samples obtained in the depth evolution experiment precludes a detailed analysis of metabolomic responses to changes in light intensity (supplementary information 6).

To explore the generality of metabolomic responses, samples collected from the depth evolution experiment were also examined. The limited temporal replication of metabolite samples obtained in the depth evolution experiment precludes a detailed analysis of metabolomic responses to changes in light intensity (supplementary information 6). Nevertheless, marked positive correlations between the intermediates of fucose and cAMP respectively are evident (supplementary information 6) lending further support to the trends observed in the sediment overloading experiment.

Discussion:

Here we monitored the responses of cryoconite hole morphology, biogeochemistry and metabolome to changes in light intensity and sediment supply. Disturbing the light intensity at the hole floor changed the hole's depth, while sediment delivery expanded the hole floor and thinned sediment towards a SGL. Importantly, both responses stabilised carbon fluxes in the cryoconite holes, maintaining net autotrophy. In a natural setting these processes are coupled, providing a 3D biocryomorphic regulation of carbon budgets within cryoconite holes. These interactions necessitate metabolic adaptations rather than reconfiguration of the microbial community, since community doubling times exceed 10 days (Anesio et al., 2010) and recent studies have shown community structures in Greenlandic cryoconite ecosystems to be stable over weeks-months (Musilova et al., 2015; Stibal et al., 2015). Indeed, contemporary reverse-transcribed V3-V4 16S rRNA amplicon data from individual, undisturbed cryoconite holes at the study site (Site description; supplementary information)

verify the overall stability of cryoconite bacterial communities, and in particular the stable dominance of one *Cyanobacteria* OTU among the presumably active bacterial community. For ease of interpretation we discuss the processes of depth evolution and planform evolution separately, before placing our findings in the context of metabolome-level responses and carbon fixation, and their implications for glacial ecology and biogeochemistry.

Depth evolution

In this study reducing irradiance caused cryoconite hole depths to decrease. This occurred faster and to a greater extent where irradiance was more attenuated. This can be explained by the existence of a critical depth where insufficient energy is transferred vertically through cryoconite for hole floor melting to pace with surface ablation. This equilibrium depth has previously been shown to decrease during periods of lower light intensity (Gribbon, 1979). Here we show that shallowing of the filtered holes was not accompanied by any statistically significant change in hole width, causing width:depth ratios to increase over the measurement period. Increases in this ratio increase the light intensity on the hole floors (Gribbon, 1979, Cook et al., 2010). Since light is the primary driver of photosynthesis, the evolution of hole depths and the consequent impact upon photosynthesis explains the NEP convergence and the correlations between hole depth and NEP in the filtered holes. Under both filters, net autotrophy was re-established after an initial shift to net heterotrophy, suggesting that depth evolution may well be a mechanism of carbon homeostasis occurring within the cryoconite holes. The observation of persistent significant differences between NEP in each light regime has two plausible explanations. Firstly, our observation period may simply have been too short to record complete convergence. Alternatively, the filters might have established a degree of light limitation that was too great to be completely corrected by hole shallowing. These explanations are not necessarily mutually exclusive but if the latter is true, it may signify the limits of photosynthetic regulation emerging from depth equilibration alone for

these holes. We also observed some depth evolution in the overloaded cryoconite holes. A logarithmic decrease in depth in Hole 2 likely resulted from the insulating effect of MGL cryoconite with diminishing effect as the sediment spread (Wilson, 1953; Østrem, 1959). This might partly counteract the photosynthesis suppressing effect of granule overlapping. In Hole 3, depth decreased linearly to a minimum, after which the hole rapidly deepened again. This was likely a response to increased irradiance following calving of ice from heavily weathered and overhanging hole walls. Deepening in response to increased irradiance might protect hole-associated autotrophs from inhibitory light intensities (e.g. Yallop et al, 2012).

Planform evolution

While we artificially added cryoconite to existing holes, sudden high magnitude 'sediment dumps' occur in natural systems due to the merging of cryoconite holes (this natural phenomenon is illustrated in a photograph in supplementary information 1B). Where granules are stacked in thick layers in contact with the hole walls, accelerated melt causes the hole walls to recede. This creates space for granules to fall into and causes the walls to become increasingly overhung (Figure 1, also see supplementary information 1E and 1F). Consequently, this exacerbates the preferential illumination of peripheral areas of the hole floor incurred by low solar angles. Hole floor melting is therefore concentrated at the edges of the hole floor, driving slope formation (as indicated by the formation of the ER: Figure 3A). As hole walls continue to recede, hole floor slopes increase towards the periphery, causing the ER to contract. An outer zone of sloping hole floor, occupied by thinner granule layers expands at the expense of a flat interior zone occupied by thick MGL cryoconite. This stage of equilibration entails a thinning from the periphery, although there is also downslope sliding within the outer zone maintaining contact between thick MGL cryoconite and the hole walls, which sustains lateral melt.

Wiley-Blackwell and Society for Applied Microbiology

Once the ER has contracted fully, the hole floor slopes from the centre and there are ubiquitous downslope movements of cryoconite. SGL therefore propagates outwards from the hole centre (Figure 2; Figure 3B) while MGL was sustained at the interface between cryoconite and hole walls. In Hole 3, a small area of completely bare ice developed forming a pinnacle, likely due to steep slopes. However, this rapidly melted and the bare ice was re-colonised by SGL cryoconite. Such pinnacles were also observed in undisturbed cryoconite holes at the field site (supplementary information 1C) and have previously been noted on a Canadian glacier (McIntyre, 1980), suggesting that these morphological responses are not limited to artificial disturbances.

In the latter stages of re-equilibration, increasing width:depth ratios, more uniform sediment distributions and straightening of hole walls by surface ablation reduce the heterogeneity of hole floor irradiance. Slope gradients therefore diminish and the drivers of lateral equilibration weaken. A new equilibrium state can then be attained, characterised by a wide, flat hole floor with cryoconite in an even SGL. We have developed a conceptual model to explain this process (Figure 5), which highlights maintenance and acceleration of this equilibration by two positive feedback loops. The effect of this equilibration is to minimise overlapping of granules and maximise the exposure of cryoconite autotrophs to incoming solar radiation, therefore promoting net autotrophy. This explains our NEP observations and corroborates those made by Cook et al., (2010) and Telling et al., (2012) and is further supported by our sediment thickness experiment (supplementary information 4).

We also observed a preference for holes to expand northwards, likely due to the more prolonged irradiance of south facing walls promoting net northward migration of cryoconite (Figure 2). Topographic shading from the south exacerbated this effect in Hole 1 (Figure 2). A bare ice ‘stripe’ running east to west across the width of Hole 1 developed and grew into an ice wall, eventually separating the hole into two distinct entities. The same hole’s south

facing wall invaded another smaller hole during its push northwards, resulting in a sudden 'cryoconite dump' and complicating Hole 1's evolutionary trajectory. Supplementary information 1D shows a bare ice stripe developing in an undisturbed cryoconite hole at our field site. These observations indicate that heterogeneous irradiance of the hole floor can drive cryoconite hole migration, division and coalescence, and may provide a mechanism of creep away from shady north-facing slopes towards better lit areas on the ice surface.

In both of our experiments, hole widths and depths responded non-linearly to disturbances, yet their width:depth ratios changed linearly, illustrating emergent biocryomorphic stability. Planform evolution always maximises the surface area of the hole floor and minimises the sediment layer thickness. Since hole floor irradiance and sediment layer thickness are primary controls on NEP (Cook et al., 2010; Telling et al., 2012; supplementary information 6), this presents a mechanism to promote the accumulation of organic carbon in cryoconite holes.

Non-targeted Metabolomics

We hypothesised that the responses of cryoconite microbiota would be characterized by metabolic adaptations to changes in carbon flux incurred by altered receipt of solar energy. Chemometric analysis of broad-spectrum metabolite profiles generated via non-targeted mass spectrometry confirms this hypothesis. Within the sediment overload experiment we observed a broad-scale shift in metabolic profile concomitant with the switch from net heterotrophy to autotrophy and the return to a SGL (Figure 4A). The major sources of variation over time were associated with cAMP metabolism and fucose catabolism (Figure 4B), as evidenced by correlative analyses of intermediates from KEGG-derived cAMP and fucose metabolic pathways. While the limited number of samples from the depth evolution experiment precluded detailed analyses, these trends were evident in both experiments (Figure 4 and Supplementary Data). Consequently, we contend that perturbations from SGL

and equilibrium depth are associated with shifts in fucose and cAMP metabolism. An interesting feature in the sediment overload experiment is that Hole 1 on Day 7 is an outlier in terms of its global metabolite, cAMP and fucose intermediate profiles (Figure 4 A, D-F) relative to Holes 2 and 3, and resembling the profile of MGL cryoconite (i.e. prior to equilibration). As noted above, this hole experienced a "cryoconite dump" at this point, naturally perturbing the cryoconite grain layer. This congruent "resetting" of the cryoconite load and metabolite profile lends further support to our interpretation of the metabolite dataset.

We note that deoxysugars, including fucose, are a major constituent of extracellular polysaccharides in cold-region filamentous cyanobacteria (Pereira et al., 2009), the ecosystem engineers forming cryoconite granules (Langford et al., 2010; Edwards et al., 2014). Under light-limited conditions, fucose is catabolized to pyruvate as an energy source rather than utilized in the synthesis of EPS and hence aggregation of cryoconite. Meanwhile, cAMP is a potent secondary messenger molecule (Cann, 2004). In cyanobacteria (and cyanobacterial aggregates) it is associated with the regulation of stress responses and in particular photoresponsive adaptations to low light intensity (Cann, 2004; Brehm et al., 2003; Agostoni & Montgomery, 2014) for example motility (Terauchi & Ohmori, 2004) and aggregation (Ohmori et al., 1992). Consequently, the observed decline in cAMP concomitant with the return to a SGL configuration of cryoconite is consistent with a photoresponsive adaptation to low light when sediment is overloaded. Considering the scope of cAMP-responsive cyanobacterial adaptations include processes with implication for cryoconite granule structure (viz. motility and aggregation), future work should examine granule morphology and cyanobacterial behaviour in detail during biocryomorphic evolution.

Finally, the role of dichlorophenol as a source of variation in the PCA should be noted. Previously, Stibal et al., (2010) evaluated the potential for 2,4-dichlorophenoxyacetic acid to

be mineralized by bacteria isolated from the Greenland Ice Sheet surface. Therefore, it may be that 2,4-dichlorophenoxyacetic acid is catabolized to dichlorophenol by heterotrophic bacteria associated with cryoconite.

Implications for glacier ecology and biogeochemistry

We show cryoconite NEP is resilient to changes in light regime and sediment supply (Holling, 1973). This resilience arises from the three dimensional biocryomorphic evolution of cryoconite holes towards an equilibrium state characterised by high width: depth ratios and SGL sediment arrangements. At equilibrium, the hole floor is optimised for autotrophy because photosynthesis is not limited by shading of autotrophs by overlapping granules (Cook et al., 2010; Telling et al., 2012). Hole floor irradiance is then sensitively managed via the adjustment of hole depth (Gribbon, 1979). We have shown that departures from this equilibrium state are opposed by biocryomorphic mechanisms, maintaining net autotrophy and therefore net carbon sequestration.

Since photosynthesis in cryoconite holes is controlled primarily by irradiance and granule overlapping (Cook et al., 2010; Telling et al., 2012) which is in turn modulated by biocryomorphic evolution, we expect photosynthesis to be resilient to shifts in light and sediment supply. In contrast, previous studies imply that respiration in cryoconite might resist environmental disturbances in the interior zones of the Greenland Ice Sheet. There, the dominant heterotrophs are metabolically flexible (White et al., 1996; Stibal et al., 2015) and unlikely to be limited by contemporary autochthonous OC production (Stibal et al., 2010, 2012b; Telling et al., 2012). Our data cannot be used to determine rates of photosynthesis and respiration individually because the artificial manipulation of light regime in our experiments weakens the assumption of parity between respiration in light and dark incubations (e.g. Yallop, 1982; Bender et al, 1987; Telling et al, 2010). It is not surprising that respiration was relatively constant throughout the study because the conditions in the dark incubations were

stabilised by the tin foil wrapping and daily refreshing of cryoconite and meltwater. Nevertheless, our NEP measurements clearly indicate that biocryomorphic evolution of cryoconite holes is an important and hitherto overlooked regulator of ice surface biogeochemistry.

Net carbon sequestration necessitates accumulation of autochthonous OC, which has previously been identified in the interior zones of the Greenland Ice Sheet (Stibal et al, 2012b; Telling et al, 2012). This promotes granule growth and stabilization by entangling allochthonous organic and inorganic matter and by supporting heterotrophy, resulting in the production of humic and extracellular polymeric 'cements' (Langford et al., 2010; Takeuchi et al., 2010). This has several important ecological implications: 1) granules provide stable microhabitats for diverse microbes; 2) larger granules are more likely to settle on ice surfaces for long enough to form cryoconite holes; and 3) autochthonous OC darkens these granules, exacerbating the albedo differential between granules and surrounding ice, driving hole formation (Takeuchi et al., 2001; Takeuchi et al., 2010; Tedesco et al., 2013). The persistence of low albedo, biologically-formed granules that are resistant to disaggregation is a pre-requisite for biocryomorphic evolution – a process that maintains favourable conditions for microbial life. We therefore suggest that ecosystem engineering in cryoconite holes is not limited to individual granules, but extends to the shaping of cryoconite holes. Furthermore, we identified a mechanism of creep away from shade driving division, coalescence and migration of holes, implying a degree of predictability in mesoscale cryoconite dynamics that warrants further investigation, which is of especial interest since the ubiquity of cryoconite holes on ablating ice worldwide suggests biocryomorphic shaping of supraglacial topography and the potential for ecosystem engineering of granules to propagate through to the shaping of ice surfaces at the landscape scale.

Experimental Procedures

Field Site:

Field work was undertaken 38 km inland of the margin of the south-west Greenland ice sheet at Weather station site S6 (coordinates 67°04.728' N; 49°23.911'; elevation 1010m) during the period 22nd and 30th July 2014. Test holes were located on relatively flat ice 200m north of a field camp, between two supraglacial streams ca.50 m to the east and west. The active bacterial community of undistrubed cryoconite holes at S6 during the study were consistently dominated by *Cyanobacteria*, and in particular one operational taxonomic unit affiliated to a filamentous taxon (Supplementary Information; Gokul, Cameron, Hegarty, Mur, Irvine-Fynn, Cook, Edwards; manuscript in preparation).

Light Regime:

Four sets of three cryoconite holes were selected on the basis of their similar dimensions, topographic settings, close proximity and apparent stability. From each hole in the first set, cryoconite was removed using a sterile syringe and placed in 50 ml plastic tissue culture flasks filled with meltwater and incubated on the ice surface (NBS Biologicals, Ltd. Cambridge UK). This was repeated for each hole in the second and third sets, except that the flasks were returned to the hole floors. The holes were then overlain by a "e-colour+" (Rosco, London, UK) neutral density filter. The filter covering the second set of holes had transmission 51% (termed 'weaker filter' throughout the manuscript) and the filter covering the third set of holes had transmission 13% ('stronger filter'). In the fourth set of holes, no filter was used and these samples act as a control group reflecting natural conditions. Triplicate incubations were therefore established to measure NEP in each of four light regimes: surface, natural, weaker filter and stronger filter. A 'dark' incubation was also included in each light regime. Hole dimensions were monitored at least daily using callipers, rule and tape measure with 1mm increments.

Sediment Overload:

Three pairs of cryoconite holes with similar dimensions, topographic setting and apparent stability (indicated by SGL cryoconite sediment and circular planforms) were selected. One of each pair was made the 'test hole' while the other was the 'surrogate'. Each hole and its surrogate were overloaded with cryoconite sourced from nearby holes. The volumes of cryoconite added were 300 ml, 250 ml and 400 ml for Holes 1, 2 and 3 respectively to provide equivalent loads according to differing hole sizes. Every 24 ± 1 hour from the time of overload, an aliquot of cryoconite was removed from the test holes at a constant, predefined distance from the hole centre (x). The value of x was 5, 5 and 8 cm for Holes 1, 2 and 3 respectively. The removed sediment was replaced with an equal amount of cryoconite from the equivalent location in the surrogate holes, with great care taken to recreate the original sediment arrangement. The first samples were removed along the hole's north-south axis (θ = 0). Each day, the sampling location rotated 30° clockwise. Sampling was paired such that cryoconite sampled x cm from the centre at angle θ and θ + 180° were pooled to avoid bias in productivity measurements between sectors of the hole floor. Sediment thicknesses in the test holes were recreated in the incubation flasks, which were placed in the surrogate holes to minimise disturbance in the test holes. In the test holes, sediment thicknesses were measured every 1cm from the hole centre along six radial axes every 12 ± 2 hours using a pair of graduated probes while hole dimensions were measured using callipers and a tape measure. The entire procedure was replicated in a control hole into which no sediment was added.

NEP Measurements:

In all of our experiments the well-established "ΔDIC" method (Hodson et al., 2010, Telling et al., 2010) was used to measure NEP, expressed as μg C g^{-1} d^{-1} by normalisation for time and dry mass of cryoconite. Further details are provided in Supplementary Methods.

Non-targeted metabolomics:

To gain insight into the microbial metabolic adaptations during the light regime and sediment thickness manipulation experiments, we conducted broad-range, non-targeted mass spectrometric profiling of the cryoconite metabolomes using a LTQ linear ion trap mass spectrometer (Thermo Electron Corporation). Full information is provided in Supplementary Methods.

Acknowledgements:

JMC acknowledges funding from the Gino Watkins Memorial Fund, Andrew Croft Memorial Fund and Scottish Arctic Club. AE and TI-F acknowledge Royal Society Grant (RG130314) and NERC NE/K000942/1 to AE. Dr Marek Stibal, Prof Jason Box and the Dark Snow Project team are sincerely thanked for facilitating this research by sharing camp resources in summer 2014.

References:

Agostoni, M., & Montgomery, B. L. (2014). Survival strategies in the aquatic and terrestrial world: the impact of second messengers on cyanobacterial processes. *Life,* 4(4), 745-769.

Anesio, A. M., Sattler, B., Foreman, C., Telling, J., Hodson, A., Tranter, M., & Psenner, R. (2010). Carbon fluxes through bacterial communities on glacier surfaces. *Annals of Glaciology*, 51(56), 32-40.

Bender M, Grande K, Johnson K, Williams P J LeB, Sieburth J, Pilson M, et al., (1987) A comparison of four methods for determining planktonic community production. *Limnology and Oceanography,* 32(5): 1085–1098.

Brehm, U., Krumbein, W. E., & Palińska, K. A. (2003). Microbial spheres: a novel cyanobacterial–diatom symbiosis. *Naturwissenschaften*, 90(3), 136-140.

Cann, M. J. (2004). Signalling through cyclic nucleotide monophosphates in cyanobacteria. *New phytologist*, 161(1), 23-34.

Cook J, Hodson A, Telling J, Anesio A, Irvine-Fynn T, Bellas C (2010) The mass-area relationship within cryoconite holes and its implications for primary production. *Annals of Glaciology,* 51 (56): 106-110

Cook J M, Hodson A J, Anesio A M, Hanna E, Yallop M, Stibal M, Telling J, Huybrechts P (2012) An improved estimate of microbially mediated carbon fluxes from the Greenland ice sheet. *Journal of Glaciology,* 58 (212): 1098-1108

Cook, J M, Edwards A, Takeuchi N, Irvine-Fynn TDL, (2015a) Cryoconite: the dirty biological secret of the cryosphere. *Progress in Physical Geography*. Advanced Online Publication: doi: 10.1177/0309133315616574

Cook, J M, Edwards A, Hubbard, A.L. (2015b) Biocryomorphology: Integrating Microbial Processes with Ice Surface Hydrology, Topography, and Roughness. *Frontiers in Earth Science*. 3:78

Edwards A, Anesio A M, Rassner S S, Sattler B, Hubbard B, Perkins W T, Young M, Griffith G (2011) Possible interactions between bacterial diversity, microbial activity and supraglacial hydrology of cryoconite holes in Svalbard. *ISME Journal,* 51 (1): 150-160

Edwards A, Pachebat J A, Swain M, Hegarty M, Hodson A J, Irvine-Fynn T, Rassner S M E, Sattler B. (2013) A metagenomic snapshot of taxonomic and functional diversity in an alpine glacier cryoconite ecosystem. *Environmental Research Letters,* 8 (035003)

Edwards A, Mur L, Girdwood S, Anesio A, Stibal M, Rassner S, Hell K, Pachebat J, Post B, Bussell J, Cameron S, Griffith G, Hodson A (2014) Coupled cryoconite ecosystem structure-function relationships are revealed by comparing bacterial communities in Alpine and Arctic glaciers. *FEMS Microbial Ecology,* 89 (2): 222-237

Fountain A G, Tranter M, Nylen T H, Lewis K J, Meuller D R (2004) Evolution of cryoconite holes and their contribution to melt-water runoff from glaciers in the McMurdo

Dry Valleys, Antarctica. *In* Priscu, J.C. (ed) Ecosystem dynamcs in a polar desert: the McMurdo Dry Valleys, Antarctica, *Washington, DC: American Geophysical Union,* 323-335

Gribbon P W (1979) Cryoconite holes on Sermikavsak, West Greenland. *Journal of Glaciology,* 22: 177-181

Hodson A J, Anesio A M, Ng F, Watson R, Quirk J, Irvine-Fynn T et al., (2007) A glacier respires: quantifying the distribution and respiration CO2 flux of cryoconite across Arctic supraglacial ecosystem. *Journal of Geophysical Research,* 112 (G4): G04S36

Hodson A, Anesio A M, Tranter M, Fountain A, Osborn M, Priscu J, Laybourn-Parry J, Sattler B (2008) Glacial Ecosystems. *Ecological Monographs,* 78 (1): 41-67

Hodson A J, Bøggild C, Hanna E, Huybrechts P, Langford H, Cameron K, Houldsworth A (2010) The cryoconite ecosystem on the Greenland ice sheet. *Annals of Glaciology,* 51 (56): 123-129

Holling C S (1973) Resilience and stability of ecological systems. *Annual Review of Ecology and Systematics,* 4: 1-23

Hood E, Berner, L (2009) Effects of changing glacial coverage on the physical and biogeochemical properties of coastal streams in southeastern Alaska. *Journal of Geophysical Research*, 114, G03001, doi:10.1029/2009JG000971.

Kohshima S (1987) Glacial biology and biotic communities. *In:* Kawano. S., Connell, J.H., Hidaka, T. (eds), *Evolution and Coadaptation in Biotic Communities, Faculty of Science, Kyoto university,* 77-92

Kohshima S, Seko K, Yoshimura Y (1993) Biotic acceleration of glacier melting in Yala Glacier, Langtang region, Nepal Himalaya. *IAHS Publication 218 (Symposium at Kathmandu 1992 – Snow and Glacier Hydrology):* 309 – 316

Langford H, Hodson A, Banwart S, Bøggild C (2010) The microstructure and biogeochemistry of Arctic cryoconite granules. *Annals of Glaciology,* 51 (56): 87-94

Lawson E C, Wadham J L, Tranter M, Stibal M, Lis G P, Butler C E H, Laybourn-Parry J, Nienow P, Chandler D, Dewsbury P (2014) Greenland ice sheet exports labile organic carbon to the Arctic oceans. *Biogeosciences,* 11, 4015-4028

McIntyre N F (1980) Cryoconite hole dynamics. *MSc Thesis, St John's College, Cambridge, 1980*

McIntyre N F (1984) Cryoconite hole thermodynamics. *Canadian Journal of Earth Science,* 21: 152-156

Musilova, M., Tranter, M., Bennett, S. A., Wadham, J., & Anesio, A. M. (2015). Stable microbial community composition on the Greenland Ice Sheet. *Frontiers in microbiology,* 6:193

Ohmori, K., Hirose, M., & Ohmori, M. (1992). Function of cAMP as a mat-forming factor in the cyanobacterium *Spirulina platensis*. Plant and cell physiology, 33(1), 21-25.

Østrem G (1959) Ice melting under a thin layer of moraine, and the existence of ice cores in moraine ridges. *Geografiska Annaler, Series A,* 41: 228-230

Pereira, S., Zille, A., Micheletti, E., Moradas-Ferreira, P., De Philippis, R., & Tamagnini, P. (2009). Complexity of cyanobacterial exopolysaccharides: composition, structures, inducing factors and putative genes involved in their biosynthesis and assembly. *FEMS Microbiology Reviews*, 33(5), 917-941.

Philipp H (1912) Uber die beziehungen der kryokonitlocher zu den Schmelzschalen und ihren Einfluss auf die ablationsverhaltnisse arktische glatscher. *Zeitschrift der Geologischen Gesellschaft,* 64 (11): 489-505

R Core Team (2014) R: A Language and Environment for Statistical Computing. R Foundation for Statistical Computing, Vienna, Austria. http://www.R-project.org/

Six J, Bossuyt H, Degryze S, Denef K (2004) A history of soil research on the link between (micro)aggregates, soil biota, and soil organic matter dynamics. *Soil and Tillage Research,* 79: 7-31

Stibal M, Lawson E C, Lis G P, Mak K M, Wadham J L, Anesio A M (2010) Organic matter content and quality in supraglacial debris across the ablation zone of the Greenland ice sheet. *Annals of Glaciology,* 51 (56): 1-8

Stibal M, Sabacka M, Zarsky J (2012a) Biological processes on glacier and ice sheet surfaces. *Nature Geoscience,* 5: 771-774

Stibal M, Telling J, Cook J, Mak K M, Hodson A, Anesio A M (2012b) Environmental controls on microbial abundance on the Greenland ice sheet: a multivariate analysis approach. *Microbial Ecology,* 63: 74-84

Stibal, M., Bælum, J., Holben, W. E., Sørensen, S. R., Jensen, A., & Jacobsen, C. S. (2012c). Microbial degradation of 2, 4-dichlorophenoxyacetic acid on the Greenland ice sheet. *Applied and Environmental Microbiology,* 78(15), 5070-5076.

Stibal M, Schostag M, Cameron K A, Hansen L H, Chandler D M, Wadham J L, Jacobsen C S (2015) Different bulk and active microbial communities in cryoconite from the margin and interior of the Greenland ice sheet. *Environmental Microbiology Reports,* doi: 10.1111/1758-2229.12246

Takeuchi N, Kohshima S, Goto-Azuma K, Koerner R M (2001) Biological characteristics of dark coloured material (cryoconite) on Canadian Arctic glaciers (Devon and Penny ice caps). *Memoirs of the National Institute of Polar Research, Special Issue,* 54: 495-505

Takeuchi N, Nishiyama H, Li Z (2010) Structure and formation process of cryoconite granules on Urumqi glacier No.1, Tien Shan, China. *Annals of Glaciology,* 51 (56): 9-14

Tedesco M, Foreman C M, Anton J, Steiner N, Schwartzmann T (2013) Comparative analysis of morphological, mineralogical and spectral properties of cryoconite in Jakobshavn Isbrae, Greenland, and Canada Glacier, Antarctica. *Annals of Glaciology,* 54(63): 147-157

Telling J, Anesio A M, Hawkings J, Tranter M, Wadham J L, Hodson A J, Irvine-Fynn T D L, Yallop M L (2010) Measuring rates of gross photosynthesis and net community production in cryoconite holes: a comparison of field methods. *Annals of Glaciology,* 51 (56): 135-144

Telling J, Anesio A M, Tranter M, Stibal M, Hawkings J, Irvine-Fynn T D I, Hodson A, Butler C, Yallop M, Wadham J (2012) Controls on the autochthonous production and respiration of organic matter in cryoconite holes on high Arctic glaciers. *Journal of Geophysical Research,* 117 (G01017)

Terauchi, K., & Ohmori, M. (2004). Blue light stimulates cyanobacterial motility via a cAMP signal transduction system. *Molecular Microbiology*, 52(1), 303-309.

West N E (1990) Structure and function of microphytic soil crusts in wildland ecosystems of arid to semi-arid regions. *Advances in Ecological Research*, 20, 179–223

Wharton R A, McKay C P, Simmons G M, Parker B C (1985) Cryoconite holes on glaciers. *BioScience,* 35: 449-503

White D C, Sutton S D, Ringelberg D B (1996) The genus *Sphingomonas:* physiology and ecology. *Current Opinion in Biotechnology,* 7: 301-306

Wilhelm L, Singer G A, Fasching C, Battin T J, Besemer K (2013) Microbial biodiversity in glacier-fed streams. *ISME Journal,* 7: 1651 – 1660

Wilson J W (1953) The initiation of dirt cones on snow. *Journal of Glaciology,* 2: 281-287

Yallop M L (1982) Some effects of light on algal respiration and the validity of the light and dark bottle technique for measuring primary productivity. *Freshwater Biology*, 12 (5): 427–433.

Yallop M L, Anesio A J, Perkins R G, Cook J, Telling J, Fagan D, MacFarlane J, Stibal M, Barker G, Bellas C, Hodson A, Tranter M, Wadham J, Roberts N W (2012) Photophysiology and albedo-changing potential of the ice-algal community on the surface of the Greenland ice sheet. *ISME Journal,* 6: 2302 – 2313

Figure Captions:

Figure 1: A) Mean NEP in the overloaded holes over the observation period. B) Hole floor diameter for each overloaded hole over the observation period. C) NEP over the observation period for each of the four light regimes. D) Hole depth over the observation period (plot legend shared with C). All error bars are one standard deviation.

Figure 2: Four sequential snapshots of hole planform and sediment distribution along six radial axes, and North-South cross sections through the sediment layer for each overloaded hole. The expansion of the hole circumference is clearly illustrated along with both the 'thinning from the edges' and 'thinning from the centre' phases of biocryomorphic evolution. 'X' markers show the hole's centroid. The right-most frame in each row show cross-sections through the sediment layer at the same four time steps. Initially the sediment is thickest in the centre and thinner at the edges, then this pattern is reversed during the second phase of evolution. All sediment layers equilibrate to relatively uniform SGLs. Thicker sediment layers towards the right-hand side of each cross-section is explained by northwards migration of sediment due to uneven irradiance. Mapping of the hole floors and spatial analyses were performed with bespoke R scripts (R Core Team, 2014; Supplementary Information 7).

Movies showing the complete time series of plan-view and cross-sectional hole shape and sediment layer evolution are available in Supplementary Information 2 and 3 respectively.

Figure 3: A) Photograph of a portion of equilibrating sediment during the "thinning from periphery" phase. i) shows the thinning peripheral cryoconite that has slid downslope into the new space created by hole wall recession; ii) shows the scarp face or 'ER'; iii) shows the thickly stacked central bulk of cryoconite. B: The same hole photographed during the subsequent "thinning from the centre" phase of biocryomorphic evolution. a) highlights the position of some air bubbles at the water surface that should not be mistaken for bare ice at the hole floor; b) shows a clear patch of very thin cryoconite coverage, where bright areas represent bare ice between granules; c) highlights that the edges of the hole floor are obscured by the overhanging hole walls. The camera and the author's blue nitrile gloves are also visibly reflected in the melt water overlying the cryoconite sediment. Although care was taken to minimise this, some reflection was unavoidable.

Figure 4: Non-targeted metabolomics reveals concomitant changes in cAMP and fucose metabolism in response to sediment overload A): Hierarchical cluster analysis showing elevated metabolite concentrations during heterotrophy relative to autotrophic conditions B): PC loadings revealing the key sources of variation: fucose, cAMP, UMP and dichlorophenol C) Heatmap based (Pearson's) correlation profile of fucose catabolism showing strong correlations between fucose metabolism intermediate concentrations D) Heatmap showing upregulation of fucose catabolites during net heterotrophy with decline upon return to net autotrophy E) Heatmap based (Pearson's) correlation profile of cAMP metabolism showing strong correlations between cAMP metabolite concentrations F) Heatmap showing upregulation of cAMP during net heterotrophy with decline upon return to net autotrophy.

Figure 5: Flow diagram illustrating the proposed mechanism of lateral equilibration, including two clearly marked positive feedback loops: Loop A and Loop B.

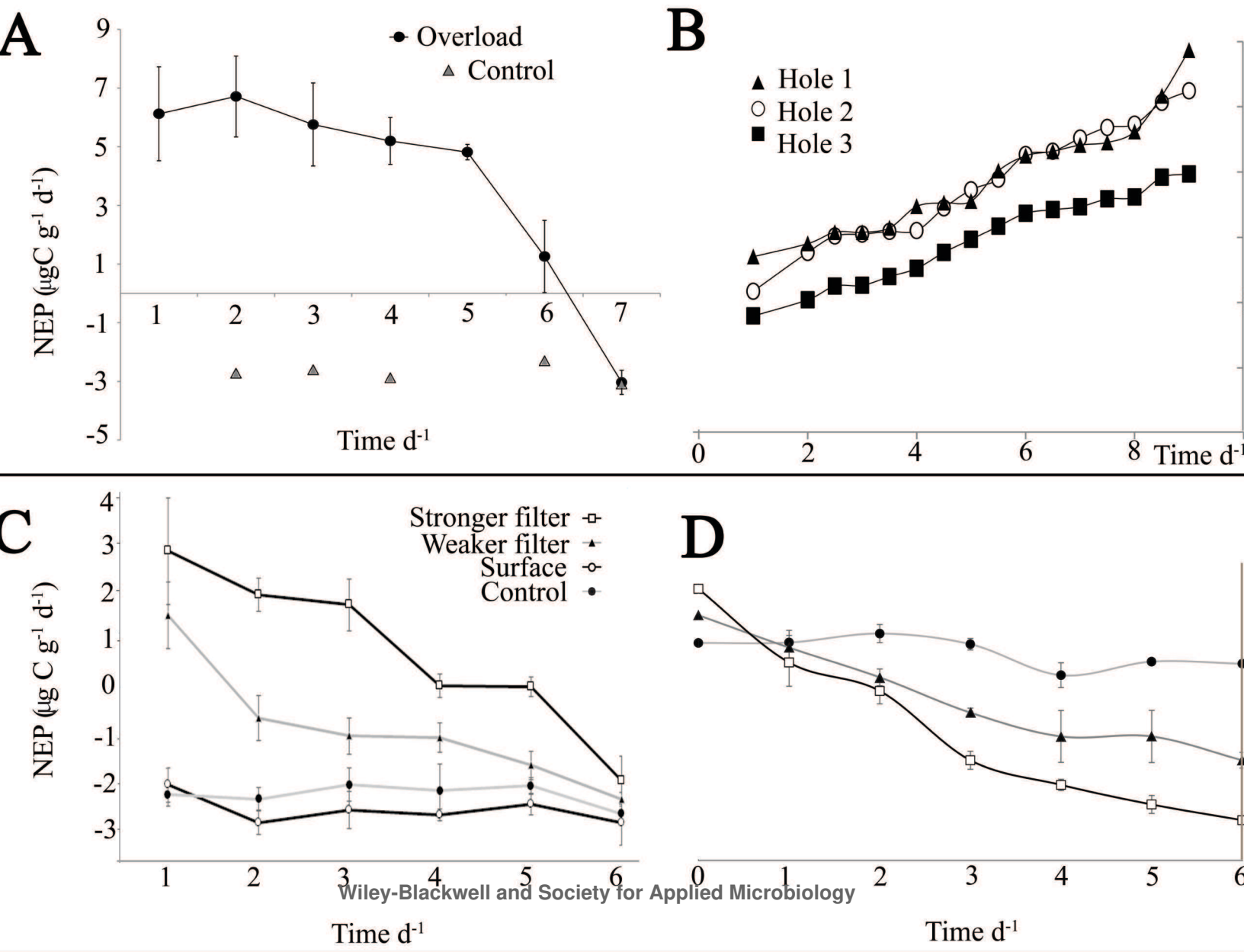

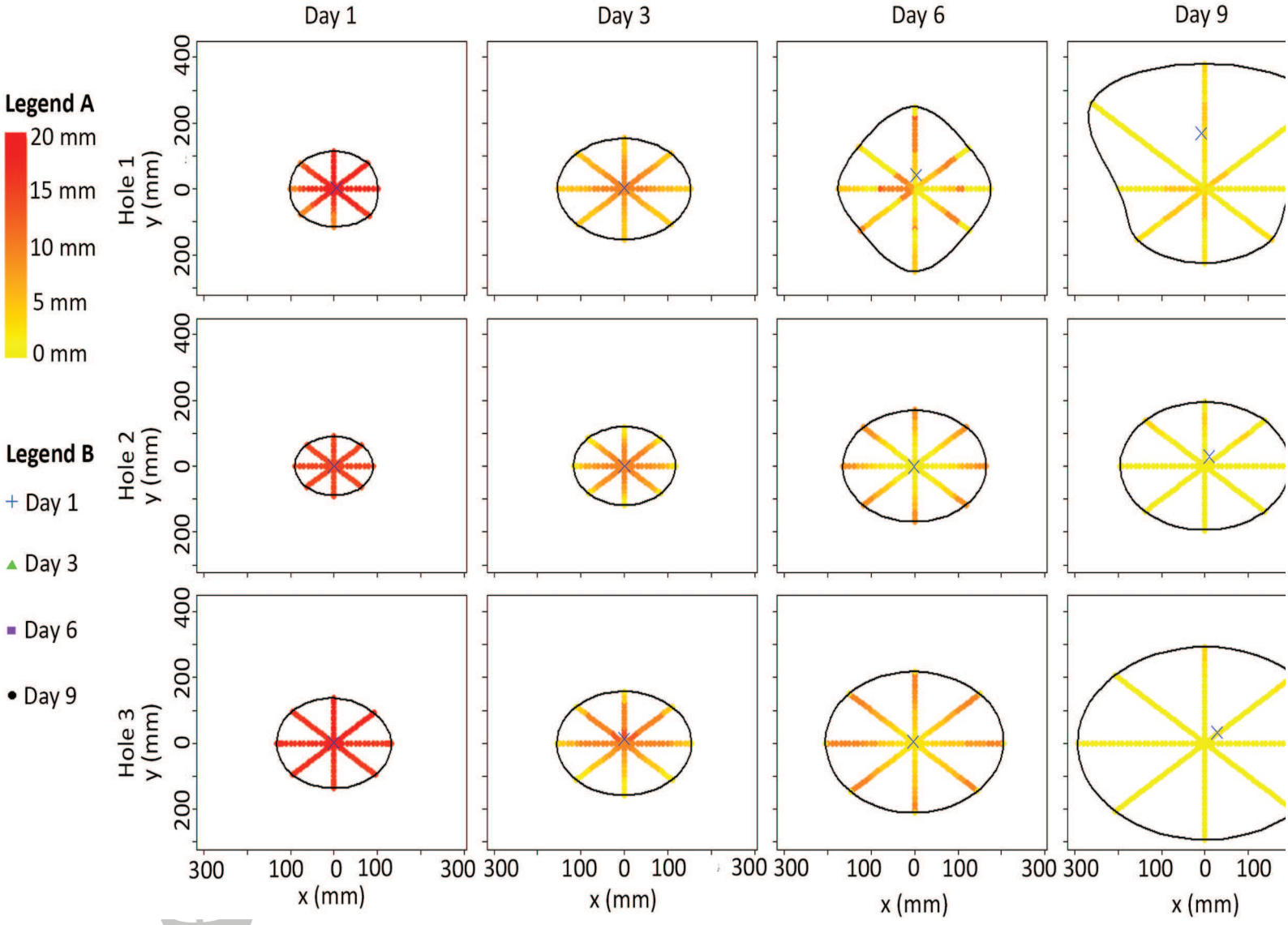

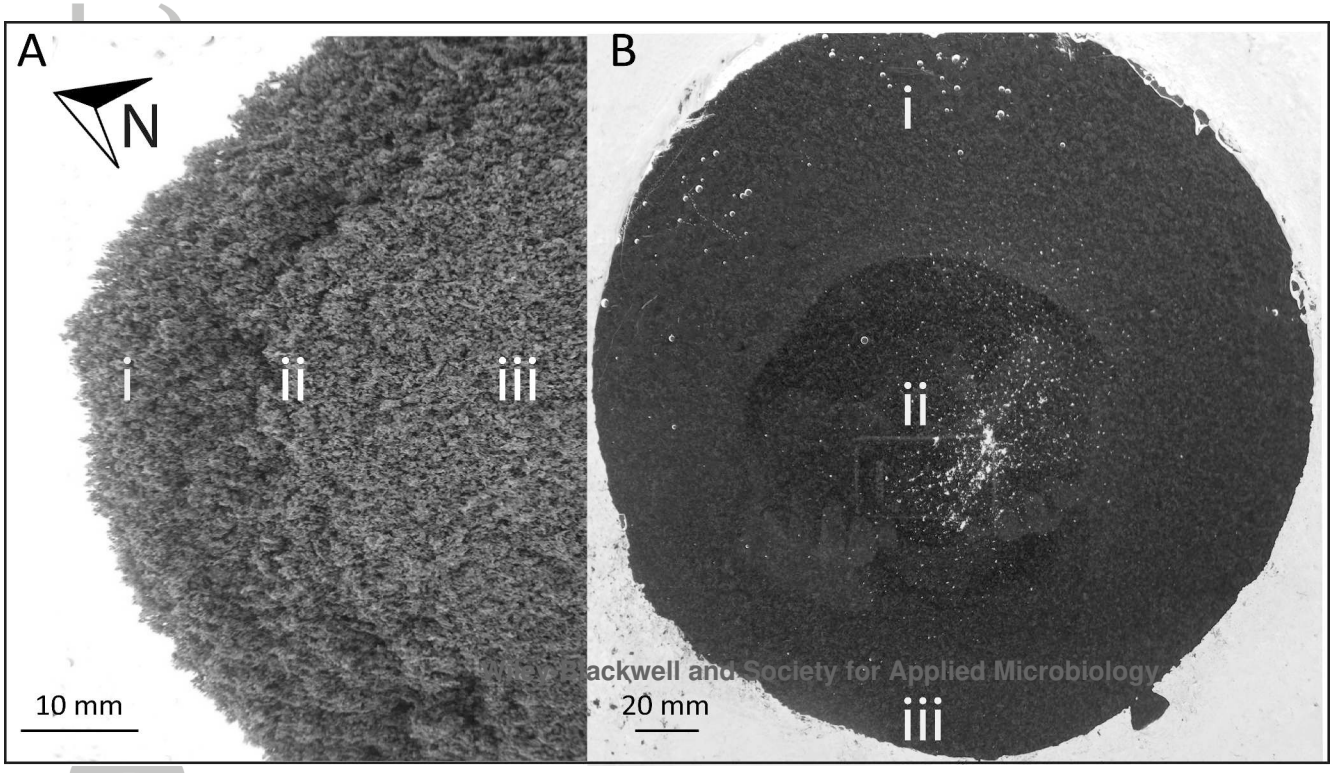

(**A**) Hierarchical Cluster Analysis of Global Metabolite Variation

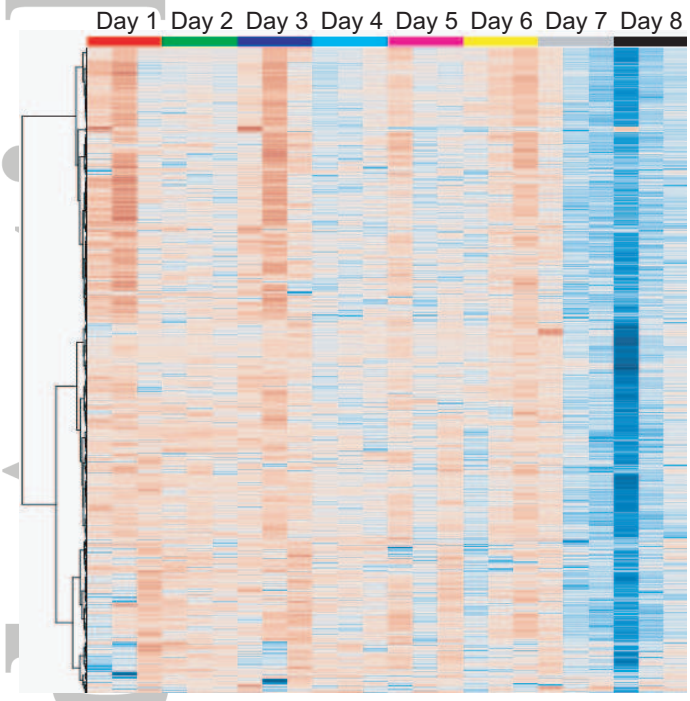

(**B**) PC-DFA Loadings from Global Analysis

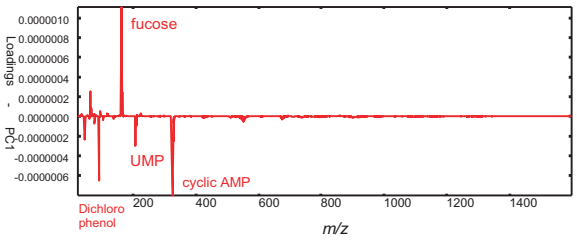

(**C**) Pearson's Correlation of Fucose Catabolism

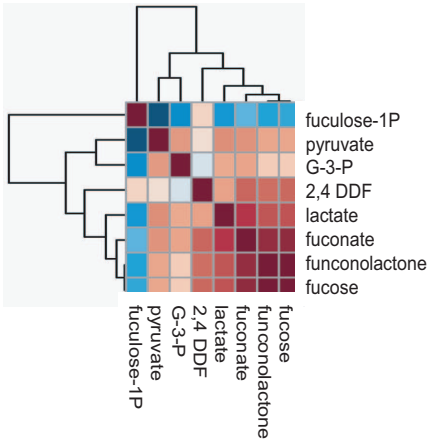

(**D**) Heatmap Analysis of Fucose Catabolism

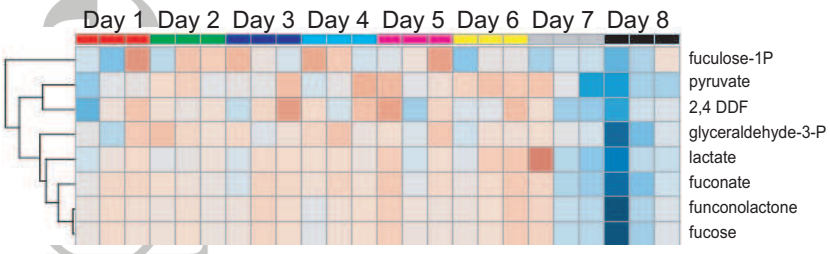

(**E**) Pearson's Correlation of cAMP Catabolism

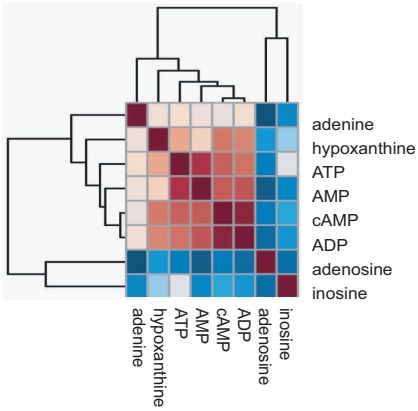

(**F**) Heatmap Analysis of cAMP Metabolism